Observation-Based Estimates of Surface Cooling Inhibition by Heavy Rainfall under Tropical Cyclones

Nicolas C. Jourdain, Matthieu Lengaigne, Jérôme Vialard, Gurvan Madec, Christophe E. Menkès, Emmanuel M. Vincent, Swen Jullien, Bernard Barnier

Observation-Based Estimates of Surface Cooling Inhibition by Heavy Rainfall under Tropical Cyclones

NICOLAS C. JOURDAIN,[*,+] MATTHIEU LENGAIGNE,[#,@] JÉROME VIALARD,[#] GURVAN MADEC,[#,&] CHRISTOPHE E. MENKES,[#,**] EMMANUEL M. VINCENT,[#] SWEN JULLIEN,[++] AND BERNARD BARNIER[+]

[+] *Laboratoire des Ecoulements Géophysiques et Industriels, Centre National de la Recherche Scientifique, Grenoble, France*
[#] *Laboratoire d'Océanographie et du Climat: Expérimentation et Approches Numériques, CNRS/IRDN/UPMC/MNHN, Paris, France*
[@] *National Institute of Oceanography, Goa, India*
[&] *National Oceanographic Center, Southampton, United Kingdom*
[**] *Institut de Recherche pour le Développement, Nouméa, New Caledonia*
[++] *Laboratoire d'Etudes en Géophysique et Océanographie Spatiale, Toulouse, France*

(Manuscript received 8 May 2012, in final form 17 September 2012)

ABSTRACT

Tropical cyclones drive intense ocean vertical mixing that explains most of the surface cooling observed in their wake (the ''cold wake''). In this paper, the authors investigate the influence of cyclonic rainfall on the cold wake at a global scale over the 2002–09 period. For each cyclone, the cold wake intensity and accumulated rainfall are obtained from satellite data and precyclone oceanic stratification from the Global Eddy-Permitting Ocean Reanalysis (GLORYS2). The impact of precipitation on the cold wake is estimated by assuming that cooling is entirely due to vertical mixing and that an extra amount of energy (corresponding to the energy used to mix the rain layer into the ocean) would be available for mixing the ocean column in the hypothetical case with no rain. The positive buoyancy flux of rainfall reduces the mixed layer depth after the cyclone passage, hence reducing cold water entrainment. The resulting reduction in cold wake amplitude is generally small (median of 0.07 K for a median 1 K cold wake) but not negligible (>19% for 10% of the cases). Despite similar cyclonic rainfall, the effect of rain on the cold wake is strongest in the Arabian Sea and weak in the Bay of Bengal. An analytical approach with a linearly stratified ocean allows attributing this difference to the presence of barrier layers in the Bay of Bengal. The authors also show that the cold wake is generally a ''salty wake'' because entrainment of subsurface saltier water overwhelms the dilution effect of rainfall. Finally, rainfall temperature has a negligible influence on the cold wake.

1. Introduction

While Tropical Cyclone (TC) track forecasts have steadily improved over the last 20 years, there has been little improvement of TC intensity forecasts (DeMaria et al. 2007). Past studies have pointed to several important physical processes that may induce uncertainties in intensity forecasts: storm inner core dynamics, structure of the atmospheric synoptic-scale environment, and air–sea interactions (Marks and Shay 1998; Emanuel 2000). The ocean surface can influence the storm intensity in mainly two ways: first, high ambient sea surface temperature (SST) ahead of the storm allows for potentially stronger storms; second, the ocean surface cooling induced by the storm may reduce enthalpy fluxes toward the atmosphere and, hence, provide a negative feedback to the storm development (Chang and Anthes 1978; Schade and Emanuel 1999; Schade 2000; Bender and Ginis 2000; Cione and Uhlhorn 2003; Kaplan and De Maria 2003). The results of Schade (2000) suggest that cyclone intensity is most sensitive to cooling under the storm, hence providing a strong incentive to better understand this cooling (referred to as the ''cold wake'' in many studies).

In situ observations of individual TCs (e.g., Jacob et al. 2000; D'Asaro et al. 2007) or numerical case studies (e.g., Price 1981; Greatbatch 1983) suggest that vertical mixing associated with the intense TC wind forcing is responsible

* Current affiliation: University of New South Wales, Sydney, New South Wales, Australia.

Corresponding author address: Nicolas C. Jourdain, CCRC, Mathews Building, Level 4, University of New South Wales, Sydney, NSW 2052, Australia.
E-mail: nicolas_jourdain@yahoo.fr

DOI: 10.1175/JPO-D-12-085.1

for 70%–85% of the SST cooling. This vertical mixing largely results from the intense vertical shear related to the strong inertial currents driven by TCs (Price 1983; Greatbatch 1984; D'Asaro 1985; Shay et al. 1989; Price et al. 1994; D'Asaro et al. 1995; Crawford and Large 1996; Tsai et al. 2008; Samson et al. 2009; Jullien et al. 2012). Recently, Vincent et al. (2012a) have confirmed that vertical mixing is the dominant cooling process close to cyclone tracks and for strong cyclones by using an ocean general circulation model to study the cold wake of more than 3000 TCs over the last 30 years. Air–sea fluxes (i.e., strong latent and sensible heat fluxes due to intense TC winds) nonetheless contribute in a non-negligible way along the track of weaker storms, and lateral advection can contribute to up to 15% of the cooling for most intense TCs (Vincent et al. 2012a).

Numerous studies have been dedicated to understand how precyclone oceanic stratification may influence the cold wake. One, indeed, expects a stronger cooling by vertical mixing in regions of a steep and shallow thermocline. The parameter that has so far been used to account for this subsurface oceanic control of the cold wake is upper-ocean heat content (OHC): the heat content above the 26°C isotherm. The fact that the OHC only brought moderate 5% improvements to statistical forecasts of cyclone intensity (DeMaria et al. 2005; Mainelli et al. 2008) or that enthalpy fluxes extracted by TCs are always a small fraction of the OHC (Cione and Uhlhorn 2003) has, however, prompted authors to propose better-suited metrics of air–sea interaction under TCs. Price (2009), for example, has proposed the upper 100-m averaged temperature T_{100} as a metric, on the basis that the typical vertical mixing depth of TCs is 100 m. More recently, Vincent et al. (2012b) have developed the physically based cooling inhibition index (CI), a proxy of the potential energy change associated with vertical mixing of the water column. Using this metric, they show that the upper-ocean stratification can modulate the amplitude of the cooling by an order of magnitude for a given wind energy input.

Salinity stratification can also influence the cold wake. The stable salinity stratification generally found in the tropics tends to inhibit vertical mixing. In the most extreme case, a salinity stratification can exist in a nearly isothermal layer: this is called a barrier layer (Godfrey and Lindstrom 1989; Sprintall and Tomczak 1992). When a barrier layer is present, mixing first has to break through the salinity-stratified layer before it can entrain colder water from below and cool the ocean surface. Neetu et al. (2012), for instance, have demonstrated that salinity effects reduce the TC-induced cooling by 30% in the Bay of Bengal during the postmonsoon season (characterized by a very fresh surface layer and the presence of the barrier layer). Consequently, TC intensification rates are significantly higher over regions with barrier layers (Balaguru et al. 2012).

The water cycle may also influence the cold wake through the intense precipitation that often characterizes TCs. Tropical cyclone rainfall can influence SST through the rain sensible heat flux. The rain positive buoyancy flux can also affect static stability of the upper ocean, with the ability to modulate vertical mixing. To our knowledge, only Jacob and Koblinsky (2007) have investigated these effects in a case study, using a high-resolution ocean model forced by observed winds from hurricane Gilbert in the Gulf of Mexico. They have found that the stabilizing effect of rain can weaken the cold wake by 0.2 to 0.5 K locally but that the associated sensible flux only marginally influences the amplitude of the TC-induced cooling.

In the present paper, observation-based products are used to estimate the effect of precipitation on TC-induced cooling at the global scale from 2002 to 2009 (our statistical analysis includes 816 observed cyclones). We present the datasets used in this study (cyclone tracks, estimates of cooling and precipitation under TCs, estimates of the oceanic stratification ahead of the TC) in section 2. Our physical assumptions and our method to numerically estimate the impact of rainfall on individual observed cold wakes are detailed in section 3. We find that (i) the stabilizing effect of rainfall on TC-induced cooling is generally weak (a median of 0.07 K against a median cooling of 1 K); (ii) the effect of rain sensible heat flux is negligible; (iii) there are strong regional contrasts, like in the north Indian Ocean where the rainfall effect is three times larger in the Arabian Sea than in the Bay of Bengal. In section 4, we derive an analytical solution of the numerical method, described in section 3, by assuming a linearly stratified ocean. This gives an insight into the various physical processes that modulate the effect of rainfall on the cold wake, depending on the region. The sensitivity of our results to observational uncertainties and to our physical assumptions is discussed in section 5.

2. Datasets

Our study focuses on the 2002–09 period, during which the ocean reanalysis that we use is best constrained by observations from the Argo network. We briefly describe below the datasets that we use.

a. Cyclone tracks

Cyclone tracks are obtained from the International Best Track Archive for Climate Stewardship (IBTrACS) (Knapp et al. 2010). The latter consists of an objective combination of best track data from regional meteorological

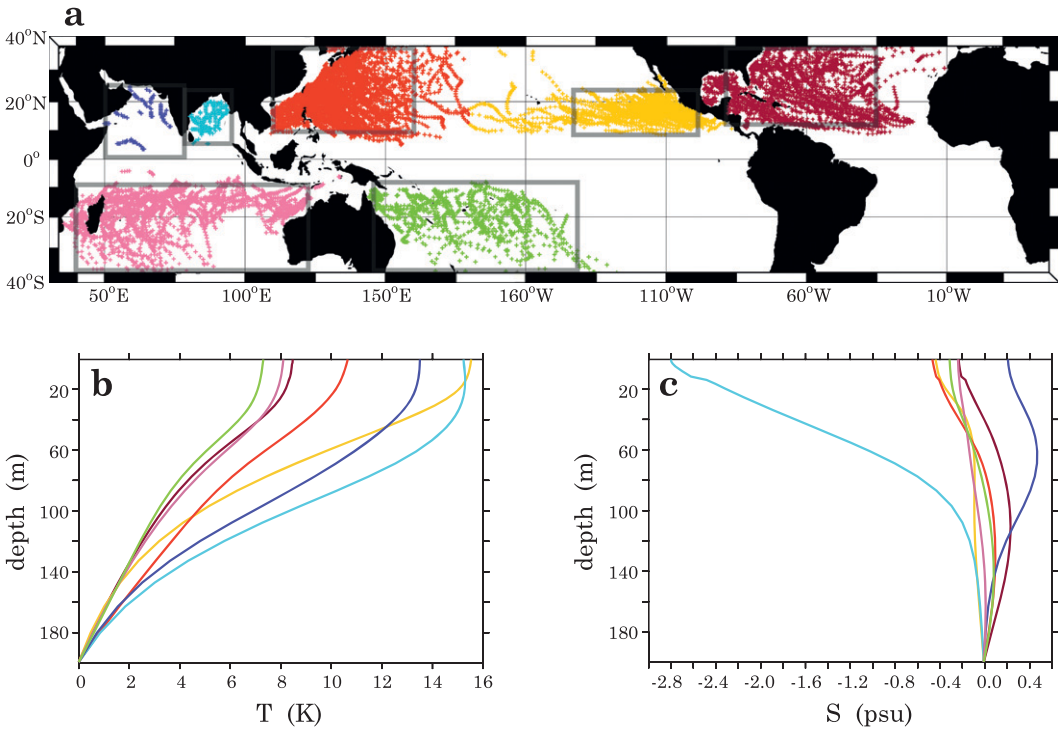

FIG. 1. (a) Individual locations (at 6-h resolution along TC tracks) considered for computations in this study, with a different color for each basin. (b) Mean GLORYS2 temperature profile during the TC season in each basin [averaged within the gray semitransparent boxes shown in (a)]. (c) As in (a),(b) but for salinity profiles. Temperature and salinity profiles are plotted as anomalies with respect to values at 200-m depth (to ease comparison between various profiles).

and warning centers at a 6-h temporal resolution. Only TCs occurring over ocean regions deeper than 250 m are considered here, and our analysis is restricted to 40°S–40°N . The statistics in this paper are based on 816 cyclone tracks with 13496 individual cyclone locations from the 6-h track data (Fig. 1a).

b. Satellite-derived TC-induced cold wake and rainfall

The SST signature in the wake of tropical cyclones is reasonably well captured by the 0.25° blended Tropical Rainfall Measuring Mission (TRMM) Microwave Imager (TMI)–Advanced Microwave Scanning Radiometer (AMSR-E) daily satellite product (see Lloyd and Vecchi 2011; Vincent et al. 2012a; Jullien et al. 2012; http://www.ssmi.com/sst/microwave_oi_sst_data_description.html). Such microwave SST estimates are relatively insensitive to cloud coverage, but do not provide reliable estimates under rainfall (Wentz et al. 2000). They do, however, provide an estimate of the cold wake, which reaches its full amplitude two or three inertial periods (2–4 days) after the TC passage (e.g., Shay et al. 1992; Jacob et al. 2000; Jullien et al. 2012; Vincent et al. 2012a; Levy et al. 2012), when satellite observations are much less affected by rain. The TC-induced SST cooling ΔSST is extracted from TMI-AMSRE after removal of the seasonal cycle. For each IBTrACS TC position, the cold wake is calculated within a 2°-radius disk as the difference between the strongest cooling after the TC (usually 1 day to 4 days after) and the SST ahead of the TC (i.e., averaged from 10 days to 2 days before the TC passage, similarly to Vincent et al. 2012b,a and Levy et al. 2012). Figure 2a illustrates the probability density function (PDF) of ΔSST for the 13 496 locations considered in this paper. The most commonly occurring TC-induced cooling is 0.5 K, while the median value is 1 K. Cooling above 3 K are rare in our dataset and they never exceed 5 K.

The TRMM 0.25° 3B42 daily product (http://disc.sci.gsfc.nasa.gov/precipitation/documentation/TRMM_README/TRMM_3B42_readme.shtml) is used to estimate accumulated rainfall under cyclones. This product is a blend of TRMM multisatellite precipitation analysis and of rainfall geostationary infrared observations when the former is not available. It is calibrated to match monthly satellite/rain gauge analyses. This product has already been used to estimate rainfall under TCs by Jiang and Zipser (2010) and Hu and Meehl (2009), and is

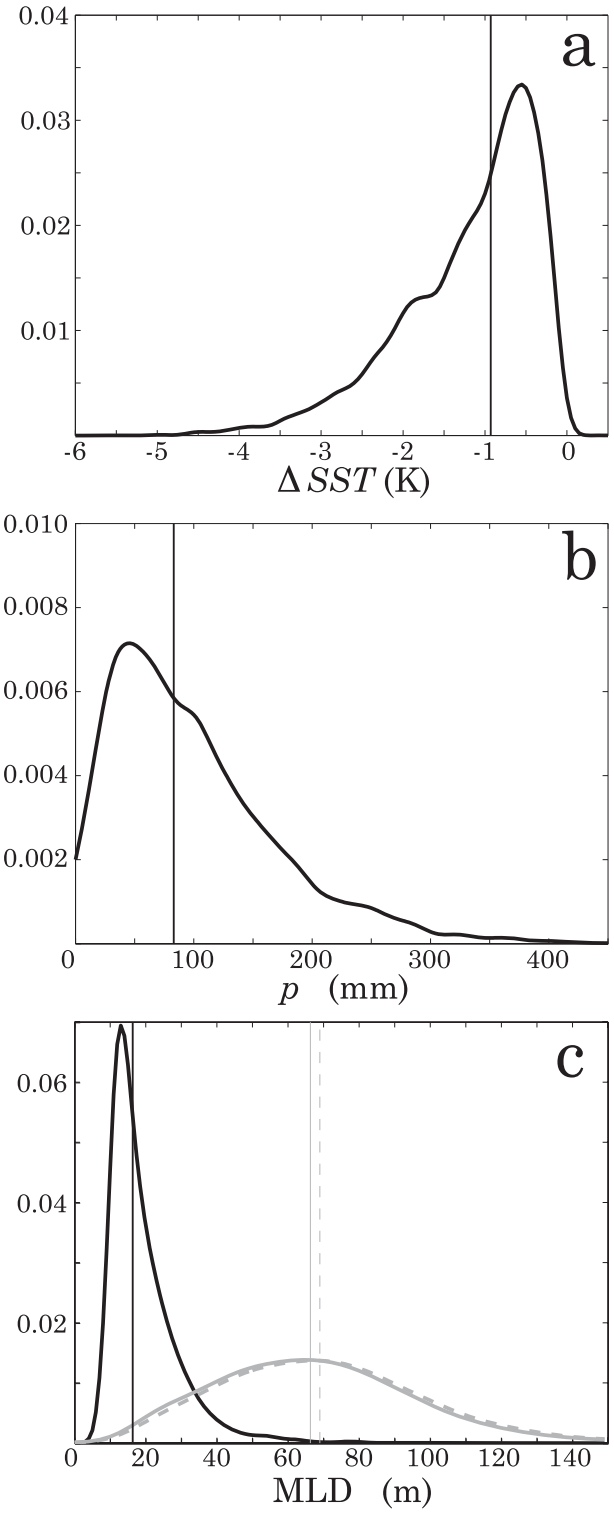

FIG. 2. Normalized probability density function of (a) TC cold wake estimated from TMI-AMSRE data, (b) cumulated TC rainfall anomalies extracted from TRMM-3B42 data, (c) MLD before the TC passage estimated from GLORYS2 (solid black), after the TC passage (solid gray, calculated from GLORYS2, see section 3), and after the TC passage in the virtual case with no rainfall (dashed gray). Thin lines indicate the median of each distribution. The PDFs are computed by attributing identical Gaussian functions to every value and adding them up [with Gaussian standard deviation of 10 m, 0.1 K, and 2.5 m in (a)–(c), respectively].

used in the National Aeronautics and Space Administration Hurricane Data Analysis Tool (http://disc.sci.gsfc.nasa.gov/daac-bin/hurricane_data_analysis_tool.pl). Recently, Chen et al. (2012, manuscript submitted to *J. Geophys. Res.*) have compared TC rainfall from 3B42 daily data to gauge observations in the Pacific. The 3B42 TC rainfall has some biases on coastal and island sites but is accurate on atoll sites, suggesting that this dataset is suitable for the analysis of TC rainfall over the open ocean. We first subtract the mean seasonal cycle from the raw dataset. Then, we obtain the accumulated amount of TC-induced rainfall p from an average over a disk of 2° radius, integrated between 8 days prior and the date that matches the one used for the estimate of the cold wake amplitude (i.e., 1–4 days after the TC passage). The estimate of p is not sensitive to the starting date of the integration (no significant rainfall is induced by TCs earlier than 3–4 days prior to its passage). The PDF of p is shown in Fig. 2b. The most common occurrence is accumulated rainfall of ~5 cm within the disk of 2° radius, and the median value is 8.5 cm: p rarely exceeds 25 cm in our dataset and does not go beyond 40 cm.

c. Ocean reanalysis

Our analysis also requires a description of the oceanic stratification ahead of the cyclone (i.e., of the upper ocean temperature and salinity profiles before the cyclone passage). These profiles are obtained from the Global Eddy-Permitting Ocean Reanalysis (GLORYS2) (Ferry et al. 2012). GLORYS2 has a global coverage at 0.25° resolution with a vertical resolution ranging from 1 m near the surface to 10 m at 100-m depth. It is built from the Nucleus for European Modelling of the Ocean (NEMO) ocean general circulation model (Madec 2008), forced by 3-hourly fields from the ECMWF Interim Re-Analysis (ERA-Interim) (Simmons et al. 2007; Dee et al. 2011), with a correction of large scale precipitation (as Troccoli and Kållberg 2004) and of radiative fluxes (Verbrugge and Garric 2010). This reanalysis assimilates the Reynolds ¼° Advanced Very High Resolution Radiometer (AVHRR) SST (http://www.ncdc.noaa.gov/oa/climate/research/sst/oi-daily.php), sea level anomaly (SLA) from the multisatellite data reprocessed by the Collecte Localisation Satellites (CLS) Center (Collecte Localisation Satellites 2011) and in situ temperature (T) and salinity (S) data from the Coriolis Ocean Database

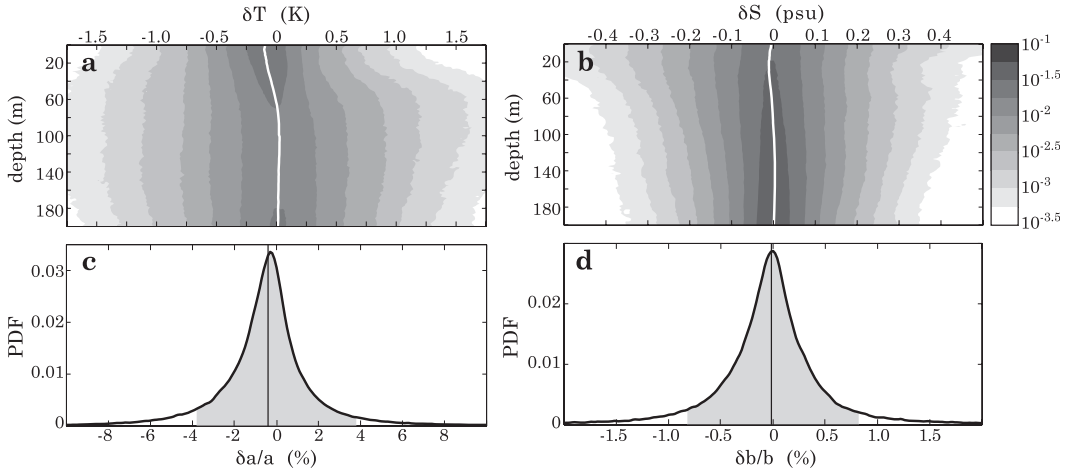

FIG. 3. (top) PDF of (a) temperature biases δT and (b) salinity biases δS in GLORYS2 with respect to ENACT/ENSEMBLE-EN3 in situ profiles (at the same day and location, considering only data in the tropical belt). The median of the distribution as a function of depth is represented by the white line. (bottom) PDF of the relative bias in the (c) linear temperature slope $\delta a/a$ and in (d) the linear salinity slope $\delta b/b$, both slopes being estimated using Eq. (13) with fixed h_m of 70 m. The gray shaded area represents 90% of the distribution of relative biases, and the vertical line shows the median of the distribution. The statistics have been calculated over the 2002–06 period for a total of 250 119 valid T profiles and 161 825 valid S profiles.

Reanalysis (CORA; www.coriolis.eu.org/Science/Data-and-Products/CORA-03). GLORYS2 cannot be used to directly evaluate the ocean response to the cyclone. This response is, indeed, strongly underestimated because the forcing dataset does not adequately resolve the very intense TC wind forcing (N. C. Jourdain et al. 2012, unpublished manuscript.) We hence only obtain the oceanic state ahead of the cyclone from this reanalysis and will explain in the next section our method to estimate the effect of rainfall on the ocean response.

Assessing the quality of the temperature and salinity profiles from GLORYS2 is a difficult task since most of the in situ hydrographic observations are assimilated in GLORYS2. We have, nonetheless, controlled that the assimilation of in situ profiles is efficient in GLORYS2. We have extracted daily temperature and salinity profiles from GLORYS2 at locations from the product EN3 provided by the projects ENACT (Enhanced Ocean Data Assimilation and Climate Prediction) and ENSEMBLES (Ensemble-Based Predictions of Climate Changes and their Impacts) hydrographic profile database (Ingleby and Huddleston 2007), following the method described by Juza et al. (2012). Figure 3a shows that the median temperature bias in GLORYS2 is −0.1 K in the first 20 m and is close to zero below 60 m depth. The median salinity bias is close to zero (Fig. 3b). Most of the T–S biases are close to the median (note the logarithmic grayscale in Fig. 3), though the spread of bias values tends to be larger between 50 and 150 m depth for T and in the first 50 m for S. There is hence only a very weak systematic bias of the GLORYS2 reanalysis at observed profiles locations. The influence of GLORYS2 uncertainties on our results will be discussed in section 5.

We use daily average estimates of the oceanic state from GLORYS2. In a consistent manner with the cold wake estimate, the precyclonic ocean state is defined as the mean profile averaged within 2° of the cyclone track between 10 and 2 days before the TC passage. Vincent et al. (2012a) underline that the oceanic mixed layer depth (MLD) is one of the important parameters in the oceanic control of the cold wake amplitude: deep MLDs request more energy input to obtain a given cooling amplitude. In this paper, MLDs are calculated as in de Boyer Montégut et al. (2004); that is, the depth at which the potential density σ_0 differs by more than 0.03 kg.m^{-3} from σ_0 at 10-m depth. The PDF of GLORYS2 MLD ahead of the cyclone passages is shown by the solid black curve in Fig. 2c. Tropical cyclones often occur in the tropics and in convergence regions where prevailing weak background winds, strong downward net heat flux, and strong rain lead to quite shallow MLDs. The most commonly occurring value in the precyclonic ocean is about 13 m, and the median value is 17 m. The MLD in TC prone regions rarely exceeds 50 m in GLORYS2.

3. Estimating the effect of rainfall on the cold wake

The first subsection below explains the physical assumptions and the numerical method that we use to estimate the effect of rainfall on the cold wake. The second subsection presents our results.

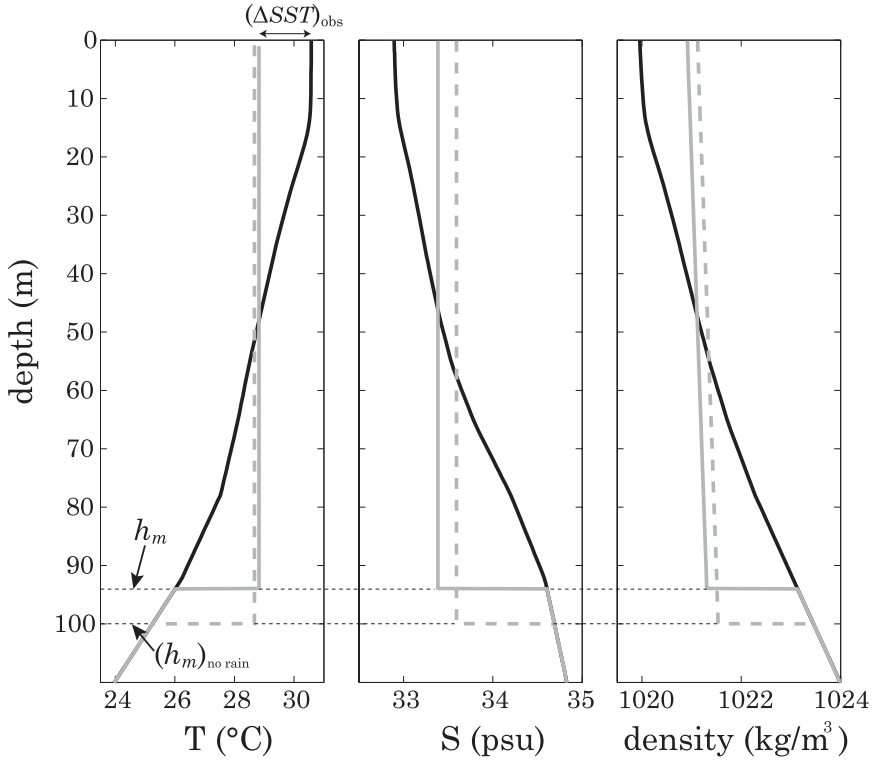

FIG. 4. Temperature, salinity, and density profiles near the location 12.5°N, 85.5°E (Bay of Bengal) corresponding to the passage of a TC on 13 May 2003 with a sustained maximum wind speed of 32 m s^{-1}, a translation speed of 2.4 m s^{-1}, and accumulated rainfall of 414 mm between t_i and t_f (from 3B42), with the assumption that $\delta T_r = 5$ K. The initial state (solid black) is from GLORYS2 with a MLD of 10 m. The final state with mixing of rain freshwater (solid gray) displays a MLD of 94 m, while the final state with no mixing of rain (dashed gray) displays a MLD of 99 m. Here $(\Delta SST)_{obs} = -1.76$ K and $(\Delta SST)_{no\ rain} = -1.91$ K.

a. Method

Our method for estimating the effect of rainfall on the cold wake is based on the same physical assumptions as in Schade and Emanuel (1999) or Vincent et al. (2012b).

- The observed cooling under TCs is assumed to be entirely due to mixing. More than 80% of the TC-induced cooling is due to mixing under slow and/or strong cyclones (e.g., Jacob et al. 2000; D'Asaro et al. 2007; Price 1981; Greatbatch 1983; Vincent et al. 2012a), so this is a reasonable assumption at first order. The consequence of such an assumption is that the total heat content of the system formed by the ocean column and the rainfall is conserved.
- The mixed layer is assumed to be perfectly homogeneous after the cyclone passage, while temperature and salinity profiles are unchanged just below (see solid gray profiles in Fig. 4). This assumption seems reasonable though it produces too sharp gradients at the base of the mixed layer.

To study the influence of rainfall, we consider that rainwater is initially a thin homogeneous layer located just above the ocean. Moreover, conservation calculations require one to define a physical system, which we choose as the system {ocean + rain}, made of the ocean water column and the rain layer. We then make three more assumptions.

- There is no evaporation so that salt is conserved if we consider that the rain layer is part of the system. The limits of this assumption are discussed in section 5.
- The rain has a salinity of zero and a temperature of SST $- \delta T_r$. No dataset is available for δT_r, but a value of 5 K is used, as estimated by Gosnell et al. (1995) and Anderson et al. (1998) in typical warm pool conditions. The sensitivity of our results to δT_r is discussed in section 5.
- The work of internal shear stress (associated with mixing) on the {ocean + rain} water column (leading to a potential energy change ΔE_p of {ocean + rain}

during the cyclone passage) would have been the same in the absence of rainfall. This assumption means that for a given initial ocean stratification ΔE_p is only driven by the TC dynamical characteristics; that is, rainfall does not strongly affect the ratio of ocean kinetic energy that is converted into potential energy. This amounts to considering that an extra quantity of energy (corresponding to the potential energy variation of the rain layer when it is mixed downward) would be available for mixing the {ocean} column in the hypothetical case with no rain.

These assumptions enable us to estimate the effect of cyclone precipitation on the cold wake following the steps below.

(i) For each TC we start from the GLORYS2 precyclonic temperature and salinity profiles (an example in the Bay of Bengal is shown by the black profiles in Fig. 4).
(ii) The postcyclone temperature profile is estimated from heat conservation, by mixing downward the initial temperature profile (rain layer included) until the SST cooling matches the TMI-AMSRE $(\Delta\text{SST})_{\text{obs}}$ (see the resulting temperature profile in solid gray, in Fig. 4). A by-product of this operation is the mixed layer depth h_m after the cyclone passage.
(iii) The postcyclone salinity (and density) profile is obtained from salt conservation by mixing downward the p-thick layer of freshwater with the initial salinity profile down to the mixed layer depth h_m (solid gray profiles in Fig. 4).
(iv) The potential energy change of the system {ocean + rain} between the precyclone and the postcyclone stratification (ΔE_p) can be calculated (it corresponds to the work exerted on the system by internal shear stress responsible for vertical mixing).
(v) The four previous steps are repeated, but, assuming that there is no precipitation, an extra quantity of energy (corresponding to the potential energy variation of the rain layer in the case it is mixed into the ocean) is available for mixing the ocean column. This enables us to obtain the postcyclone temperature and salinity profiles (dashed gray profile in Fig. 4), in the virtual case where the rain is not mixed down by the TC. The corresponding ΔSST is referred to as $(\Delta\text{SST})_{\text{no rain}}$. A by-product of this operation is the virtual postcyclone mixed layer depth $(h_m)_{\text{no rain}}$ in the absence of precipitation.

The TC-induced rain is associated with a positive buoyancy flux that partly counteracts the effect of wind-induced mixing. In the case of Fig. 4, the MLD is 5 m shallower when rainfall is taken into account, which reduces the entrainment of cold water into the mixed layer during the cyclone passage. The consequence is a weaker surface cooling when accounting for rainfall effects ($(\Delta\text{SST})_{\text{no rain}} = -1.91$ K against $(\Delta\text{SST})_{\text{obs}} = -1.76$ K). In the case of Fig. 4, the precyclonic haline stratification is stable (freshwater near the surface). The surface salinity predominant response to the TC is a saltening due to vertical mixing between the fresh surface waters and saltier thermocline waters: neglecting the effect of rain results in a higher surface salinity. This can a priori be related to both the dilution effect due to freshwater input and the slight deepening of the mixed layer when the rain buoyancy effect is neglected.

b. Influence of TC rainfall on SST

The method above allows one to estimate the effect of rainfall on the cooling amplitude for the 13496 TC-influenced 2° disks considered in the present study, with a raindrop temperature of SST − 5 K ($\delta T_r = 5$ K). The postcyclonic ocean state estimated from our method has a median MLD of 67 m (solid gray curve in Fig. 2c), which is less than the 100 m typical mixing depth considered by Price (2009), even though we obtain a closer value if we only consider hurricanes (77 m). The median MLD is 2–3 m deeper when not accounting for the rainfall effect, as shown in Fig. 2c. The median cooling inhibition due to rainfall is 0.07 K (black curve in Fig. 5a and Table 1). The 10th and 90th percentiles of the rainfall cooling inhibition are respectively 0.14 and 0.02 K. The maximum estimated inhibition is 0.34 K for the severe tropical storm Linfa, on 26 May 2003, with related p as high as 29 cm (exceptionally strong rainfall has been reported in the Philippines and in Japan at this period, Agence France-Presse 2003). These values can be compared to the observed cooling distribution in Fig. 2a. The typical effect of rainfall, measured from the median, is weak but not negligible (cooling reduction of 0.07 K) compared to the typical cooling (1 K). The typical relative cooling inhibition is 7% (median), with 80% of the values between 3% and 19% (Table 1). The cooling inhibition by rainfall is only slightly correlated to $(\Delta\text{SST})_{\text{obs}}$ (correlation of 0.22), and is moderately correlated to the rainfall p (0.43). The strongest 5% percentile of cooling inhibitions by rainfall (< -0.17 K) are all due to rainfall above the median of 8.5 cm, and half of this strongest 5% percentile is associated with the strongest 8% percentile of rainfall ($p > 21.6$ cm).

The sensitivity of our estimates to raindrop temperature is now investigated by considering the extreme case of rainfall at the same temperature as the ocean surface

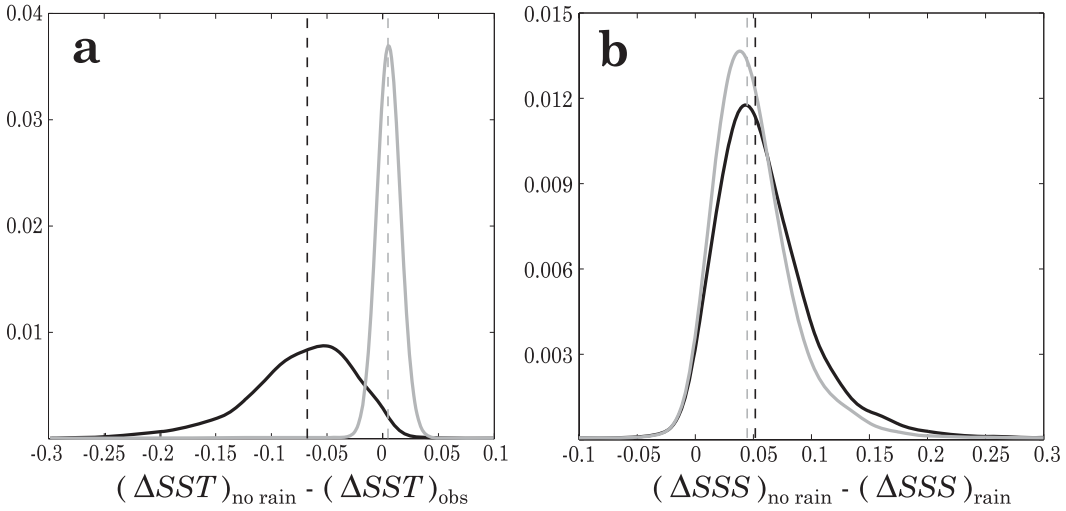

FIG. 5. (left) PDF of $(\Delta\text{SST})_{\text{no rain}} - (\Delta\text{SST})_{\text{obs}}$ and (right) PDF of $(\Delta\text{SSS})_{\text{no rain}} - (\Delta\text{SSS})_{\text{rain}}$. The solid black curve represents the PDFs calculated following the method described in section 3a, while the solid gray one represents the PDFs calculated with the assumption that the rainfall is diluted in the water column without changing the intensity of vertical mixing (i.e., the postcyclonic MLD is the same with or without rain). Here $\delta T_r = 5$ K is used to estimate the raindrop temperature.

($\delta T_r = 0$ K). As shown in Table 1, the typical change in the effect of rain is really small: about 10% of the rain effect itself (i.e., less than 1% of the cooling). The effect of rain sensible flux is hence negligible.

Two processes can be responsible for the rainfall effect on ΔSST: rainfall dilution effect or change in the penetration depth of vertical mixing. To roughly estimate the dilution effect, we have calculated the change in ΔSST that would occur if rainfall were just mixed without affecting the MLD (i.e., if $\text{MLD}_{\text{no rain}} = \text{MLD}_{\text{rain}}$). The gray curve in Fig. 5a shows that the dilution effect is rather weak and that most of the rainfall influence on the cold wake is through a change in the penetration depth of vertical mixing. We show in the following section that this change is mostly related to the positive buoyancy flux related to the input of rain freshwater.

Figure 6 provides a more detailed view of the observed TC-induced SST change (Fig. 6a) and diagnosed impact of rainfall on the SST change (Fig. 6b). Over the sample considered here, there is not a large spread of the cooling distributions in each basin (Fig. 6a). The median cooling inhibition is, however, larger in the Arabian Sea where the median value is 0.15 K, versus 0.05 to 0.09 K in other basins (Fig. 6b). The influence of rain on ΔSST is not simply proportional to ΔSST, as shown by a comparison between Fig. 6a and Fig. 6b. The simple analytical approach presented in the following section will provide some tools to explain the main factors that control rain influence on the cold wake and to explain those regional differences.

c. *Influence of TC rainfall on SSS*

The bottom panels of Fig. 6 provide an estimate of the sea surface salinity (SSS) change and impact of rainfall on SSS change in each cyclonic basin. The global median diagnosed salinity change under tropical cyclones is a saltening of 0.16 psu. This result may first appear counterintuitive owing to the large freshwater input brought by TC rainfall but can easily be explained as follows. Cyclones generally form in convective regions, where climatological rainfall leads to a stable salinity stratification (freshwater above saltier thermocline water, see Fig. 1c). The surface saltening means that most of the salinity response to cyclones is the result of vertical mixing of surface freshwater with saltier water from below, rather than the result of rain freshwater dilution. The strongest ΔSSS is found in the Bay of Bengal (Fig. 6c, median = 0.78 psu), which has a very strong salinity stratification (Fig. 1c), especially after a monsoon

TABLE 1. Median and 10th and 90th percentiles of the distributions of absolute (first row) and relative (second row) influence of rain on ΔSST, and the influence of raindrop temperature on ΔSST (third row).

		Percentile	
	Median	10th	90th
$(\Delta\text{SST})_{\text{obs}} - (\Delta\text{SST})^{\delta T_r=5\text{K}}_{\text{no rain}}$ (K)	−0.070	−0.138	−0.024
$\dfrac{(\Delta\text{SST})_{\text{obs}} - (\Delta\text{SST})^{\delta T_r=5\text{K}}_{\text{no rain}}}{(\Delta\text{SST})_{\text{obs}}}$ (%)	7	3	19
$(\Delta\text{SST})^{\delta T_r=5\text{K}}_{\text{no rain}} - (\Delta\text{SST})^{\delta T_r=0}_{\text{no rain}}$ (K)	−0.007	−0.015	−0.002

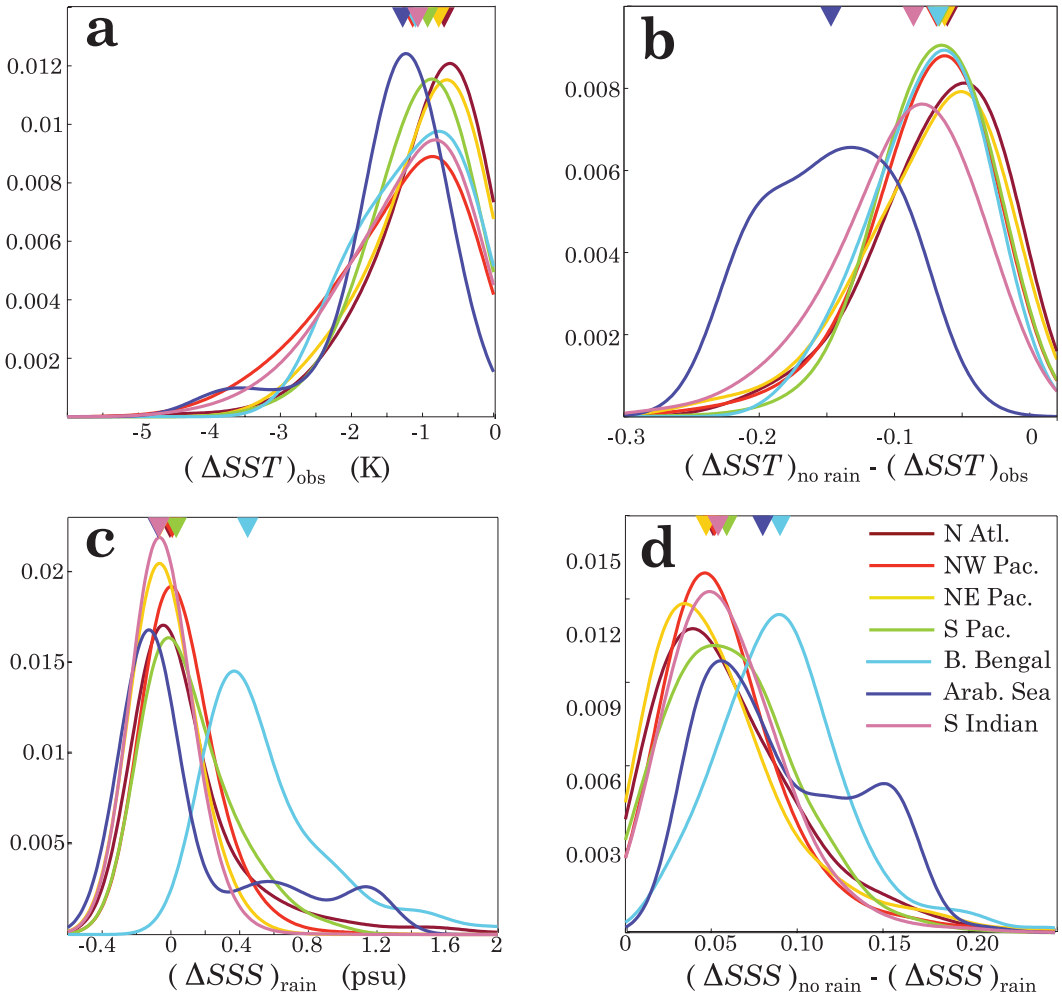

FIG. 6. (a) PDF of $(\Delta SST)_{obs}$ in various basins (from TMI-AMSRE). (b) PDF of $(\Delta SST)_{no\ rain} - (\Delta SST)_{obs}$. (c) PDF of $(\Delta SSS)_{rain}$ (calculated). (d) PDF of $(\Delta SSS)_{no\ rain} - (\Delta SSS)_{rain}$: triangles indicate median values. The PDFs are computed by attributing identical Gaussian functions to every value and adding them up.

(Neetu et al. 2012). Regions with a weaker salinity stratification in the upper 100 m, such as the Arabian Sea and the northeast Pacific, have smaller SSS response to a cyclone passage (median = 0.08 psu).

Neglecting the effect of rainfall reinforces the surface salinity increase by 0.05 to 0.1 psu (median values). As for temperature, the relative contribution of the dilution process and change in penetration depth of vertical mixing on this salinity change can be assessed by assuming that the MLD remains unchanged—accounting or not for rainfall effect (gray curve in Fig. 5b). By contrast with the effect of rainfall on ΔSST, most of the effect of rainfall on ΔSSS is a matter of dilution rather than a matter of change in the penetration depth of vertical mixing. This is probably the reason why the influence of rainfall on ΔSSS is similar in the Arabian Sea and in the Bay of Bengal, as shown in Fig. 6d (since the two basins present similar cyclonic precipitation, see section 4).

4. Analytical solution for a linearly stratified ocean

In this section, we derive an analytical solution to the numerical calculation, presented in the previous section, for the simple case of a linearly stratified ocean. This simple analytical method provides results that match well those of the numerical methods and, hence, enables the understanding of some of physical processes that lead to regional differences in the rainfall influence on the cold wake.

a. Analytical solution for the TC-induced cooling

It is assumed here that temperature $T_i(z)$ and salinity $S_i(z)$ are linearly stratified before the cyclone passage (Fig. 7):

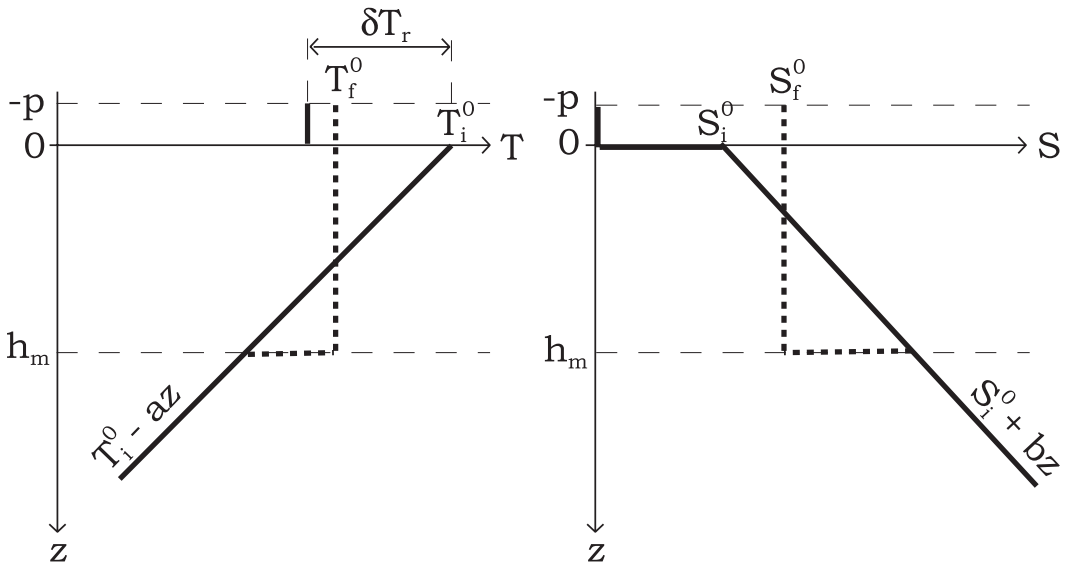

FIG. 7. Idealized T and S profiles used for the analytical computations in section 4. The thick black line corresponds to the idealized profile before the cyclone passage; the dashed line corresponds to the idealized profile after the cyclone passage.

$$\begin{cases} \left.\begin{aligned} T_i(z) &= T_i^0 - az \\ S_i(z) &= S_i^0 + bz \end{aligned}\right\} & \text{for} \quad z \geq 0 \text{ (ocean)} \\ \left.\begin{aligned} T_i(z) &= T_i^0 - \delta T_r \\ S_i(z) &= 0 \end{aligned}\right\} & \text{for} \quad -p < z < 0 \text{ (rain)} \\ a > 0, b > 0, \end{cases} \tag{1}$$

where the z axis is downward and a, b, T_i^0, and S_i^0 are constant. Given the little influence of δT_r found in the previous section, we will assume below that $\delta T_r = 0$ (a complete derivation for $\delta T_r \neq 0$ can be obtained, but is not shown here).

As in the numerical solution of the previous section, we assume that the mixed layer is perfectly homogeneous down to the depth $h_m > 0$ after the cyclone passage and that the temperature and salinity profiles are unchanged below (see Fig. 7):

$$\begin{cases} \left.\begin{aligned} T_f(z) &= T_f^0 \\ S_f(z) &= S_f^0 \end{aligned}\right\} & \text{for} \quad z \leq h_m \text{ (rain included)} \\ \left.\begin{aligned} T_f(z) &= T_i(z) \\ S_f(z) &= S_i(z) \end{aligned}\right\} & \text{for} \quad z > h_m, \end{cases} \tag{2}$$

where T_f^0 and S_f^0 are the mixed layer temperature and salinity after the cyclone passage. We assume a linear equation of state:

$$\rho(z) = \rho_0(1 - \alpha T(z) + \beta S(z)), \tag{3}$$

with α and β constant and positive. From heat conservation we obtain

$$\begin{cases} \Leftrightarrow \displaystyle\int_{h_m}^{0} (T_i^0 - az)\, dz + \int_0^{-p} T_i^0\, dz = \int_{h_m}^{-p} T_f^0\, dz \\ h_m^2 + 2\dfrac{\Delta\text{SST}}{a}(h_m + p) = 0 \end{cases}. \tag{4}$$

Equation (4) has two solutions if $2ap/\Delta\text{SST} < 1$, which is automatically true because $\Delta SST < 0$. The only physical solution (i.e., ensuring $h_m > 0$) is

$$h_m = -\frac{\Delta\text{SST}}{a}\left[1 + \sqrt{1 - 2\frac{ap}{\Delta\text{SST}}}\right]. \tag{5}$$

The final mixed layer salinity profile S_f^0 is obtained from salt conservation:

$$\begin{cases} \Leftrightarrow \displaystyle\int_{h_m}^{0} (S_i^0 + bz)\, dz = \int_{h_m}^{-p} S_f^0\, dz \\ S_f^0 = \dfrac{h_m S_i^0 + bh_m^2/2}{p + h_m}. \end{cases} \tag{6}$$

The introduction of (5) and (6) in the expression of the potential energy change ΔE_p yields

$$\frac{\Delta E_p}{\rho_0 g} = -\frac{2}{3}\tilde{N}^2\left(\frac{\Delta\text{SST}}{a}\right)^3 - p\beta S_i^0\left(\frac{\Delta\text{SST}}{a}\right), \tag{7}$$

where $\tilde{N}^2$ is the Brunt–Väisälä frequency divided by g; that is, $\tilde{N}^2 = \alpha a + \beta b$.

If p is set to zero in Eq. (7), one obtains the expression used by Vincent et al. (2012b) to develop the so-called CI index (see Introduction):

$$\Delta\mathrm{SST} = -\frac{a}{\tilde{N}^{2/3}}\left(\frac{3}{2}\frac{\Delta E_p}{\rho_0 g}\right)^{1/3}. \tag{8}$$

This equation illustrates the two competing effects of temperature on the TC-induced cooling. The term $a/\tilde{N}^{2/3}$ in Eq. (8), indeed, illustrates that (i) a strong temperature stratification makes cold water available closer to the surface and hence favors a strong $|\Delta\mathrm{SST}|$ and (ii) a strong temperature stratification tends to inhibit vertical mixing because the related density gradient tends to act as a barrier to vertical mixing.

From the above equation, two distinct regimes can be defined depending on the relative influence of the thermal and haline stratification on density:

$$\begin{cases} \text{Strong thermocline} \quad (\beta b \ll \alpha a): & \Delta\mathrm{SST} \simeq -a^{2/3}\left(\dfrac{3}{2}\dfrac{\Delta E_p}{\alpha\rho_0 g}\right)^{1/3} \\ \text{Strong halocline} \quad\;\; (\beta b \gg \alpha a): & \Delta\mathrm{SST} \simeq -\dfrac{\alpha a^{1/3}}{\beta b}a^{2/3}\left(\dfrac{3}{2}\dfrac{\Delta E_p}{\alpha\rho_0 g}\right)^{1/3}. \end{cases} \tag{9}$$

The first equation corresponds to the quite common case in which temperature largely dominates the stratification. Equation (9) shows that, in this strong thermocline limit, the effect (i) dominates; that is, a stronger temperature stratification will result in greater cooling because entrained water is colder. In the case that salinity largely controls the density stratification (i.e., in the case where there is a barrier layer, i.e., $\alpha a/\beta b \ll 1$), Eq. (9) shows that the cooling is much weaker than in the strong thermocline limit because the entrained water is almost as warm as the mixed layer.

To obtain the influence of precipitation on the cooling, we now consider the virtual case in which there is no rainfall. Assuming that the potential energy variation is the same as in the real case (as in the previous section) yields

$$(\Delta\mathrm{SST})_{\text{no rain}} = (\Delta\mathrm{SST})_{\text{obs}}\left(1 + 3\frac{\Delta_{\mathcal{B}}(-\rho g)}{\Delta_{\text{mix}}(-\rho g)}\right)^{1/3}$$

$$\text{with} \quad \begin{cases} \Delta_{\mathcal{B}}(-\rho g) = \dfrac{\mathcal{B}}{\mathcal{H}_m} = \dfrac{g\beta S_i^0 p}{\mathcal{H}_m} \\ \Delta_{\text{mix}}(-\rho g) = \dfrac{1}{2}N^2\mathcal{H}_m \\ \mathcal{H}_m = -2\dfrac{(\Delta\mathrm{SST})_{\text{obs}}}{a}. \end{cases} \tag{10}$$

As seen in Eq. (5), $\mathcal{H}_m$ represents the virtual MLD that would be found after mixing in the absence of rainfall; $\mathcal{B}$ is the time-integrated surface buoyancy flux associated with the salt dilution due to precipitation (e.g., Gill 1982). Hence, $\Delta_{\mathcal{B}}(-\rho g)$ represents the surface buoyancy change due to rainfall over an $\mathcal{H}_m$ thick layer. Similarly, $\Delta_{\text{mix}}(-\rho g)$ represents the surface buoyancy change due to mixing over the same layer layer. The second term within the left-hand brace in Eq. (10) hence represents the ratio of the rain effect on surface buoyancy to the mixing effect on surface buoyancy.

The $\Delta_{\text{mix}}(-\rho g)$ term in (10) is generally sufficiently smaller than unity (median value is ~0.2) to linearize the equation as follows:

$$(\Delta\mathrm{SST})_{\text{no rain}} - (\Delta\mathrm{SST})_{\text{obs}} = \underbrace{\frac{1}{2}\frac{g\beta S_i^0 p a^2}{N^2(\Delta\mathrm{SST})_{\text{obs}}}}_{=\mathrm{RHS}_1} = \frac{1}{\alpha g}\frac{\mathcal{B}}{\mathcal{H}_m}\frac{\alpha a}{\tilde{N}^2}. \tag{11}$$

We will demonstrate later the relevance of this linearization by comparing the approximate solution derived in this section to the numerical resolution in the previous section.

Equation (11) may be understood as follows: the term $\mathcal{B}/\mathcal{H}_m$ expresses the change of the surface buoyancy by rainfall, and the term $\alpha a/\tilde{N}^2$ tells how much the surface temperature is affected by a change of the surface buoyancy. Again, two extreme regimes can be identified:

$$\begin{cases} \text{Strong thermocline} \quad (\mathcal{B}b \ll \alpha a): & (\Delta\mathrm{SST})_{\text{no rain}} - (\Delta\mathrm{SST})_{\text{obs}} = \dfrac{1}{\alpha g}\dfrac{\mathcal{B}}{\mathcal{H}_m} \\ \text{Strong halocline} \quad\;\; (\mathcal{B}b \gg \alpha a): & (\Delta\mathrm{SST})_{\text{no rain}} - (\Delta\mathrm{SST})_{\text{obs}} = \dfrac{1}{\alpha g}\dfrac{\mathcal{B}}{\mathcal{H}_m}\dfrac{\alpha a}{\mathcal{B}b}. \end{cases} \tag{12}$$

Comparing these equations reveals that the effect of rainfall on SST is substantially weaker in the strong halocline regime (i.e., in presence of the barrier layer). This can be understood physically as follows. In the strong thermocline case, most of the potential energy change associated with mixing is used to overcome the thermal stratification, and is associated with cooling, the latter being reduced in the presence of rainfall because of the shallower mixing. In the strong halocline case, the potential energy change associated with mixing is used to overcome the haline stratification with almost no associated cooling: the rainfall inhibition will hence affect salinity more than temperature.

b. Evaluation of the linear theory

To test the validity of the analytical approach developed in this section, the numerical computation described in section 3a has been applied to linear profiles with a linear seawater equation of state. We obtained numerical results very close to the analytical solution, both for $\delta T_r = 0$ and for $\delta T_r = 5$ K (not shown), which provides some confidence in both the numerical approach and analytical computations.

The results from the linear analytical method are now confronted with those from the previous section, that is, with GLORYS2 realistic profiles and the nonlinear seawater equation of state. For each oceanic 2° disk location analyzed in section 3, we estimate an equivalent linear stratification ensuring that the heat and salt content of the linear profile is the same as the observed profile. This yields the following values of $a_{\rm obs}$ and $b_{\rm obs}$:

$$\begin{cases} a_{\rm obs} = \dfrac{2{\rm SST}_{\rm obs}}{h_m} - \dfrac{2}{h_m^2}\displaystyle\int_{h_m}^{0} T_{\rm obs}(z)\,dz \\ b_{\rm obs} = -\dfrac{2{\rm SSS}_{\rm obs}}{h_m} + \dfrac{2}{h_m^2}\displaystyle\int_{h_m}^{0} S_{\rm obs}(z)\,dz. \end{cases} \tag{13}$$

We use a constant α and β for each profile, with values computed from the Jackett and McDougall (1995) nonlinear equation of state applied to $\rm SST_{obs}$ and $\rm SSS_{obs}$.

The expression of $(\Delta{\rm SST})_{\rm no\ rain} - (\Delta{\rm SST})_{\rm obs}$ obtained in Eq. (11) is assessed using realistic profiles from GLORYS2 in Fig. 8. Even though the slope is lower than unity (0.74), the correlation of 0.85 indicates that our simple analytical approach with idealized linear profiles provides a good description of the factors controlling the TC-induced cooling in the presence of precipitation. If a and b had to be calculated in a forecasting context, that is, without knowing h_m, Eq. (11) remains valid, either by computing a and b as in Eq. (13) but with the median value of 70 m for h_m, or by computing h_m assuming a cooling of −1 K (median) to calculate h_m for every TC.

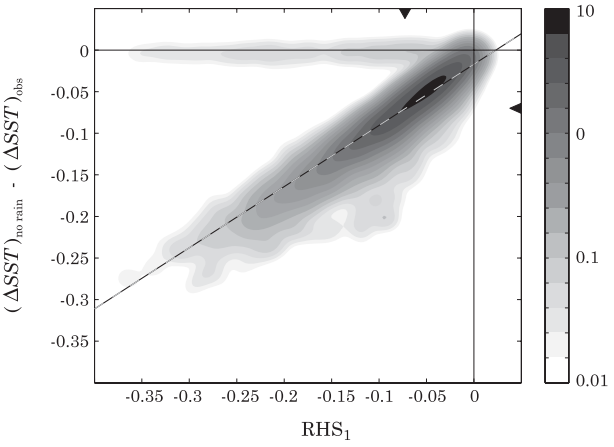

FIG. 8. PDF of $(\Delta{\rm SST})_{\rm no\ rain} - (\Delta{\rm SST})_{\rm obs}$ vs $\rm RHS_1$ [term in Eq. (11)]. The PDF is obtained by attributing identical two-dimensional Gaussian functions to every value and adding them up. The linear fit (dashed gray black) is obtained using a least-mean-square method. Black triangles indicate the median of each distribution.

The resulting correlation coefficients of 0.41 and 0.45 respectively, though highly significant, are lower than the value of 0.85 obtained above, showing the importance of describing the stratification down to the actual mixing depth.

c. Explaining regional contrasts in the rainfall effect

The term $\rm RHS_1$ from Eq. (11) is able to reproduce the regional differences in the rainfall effect on cyclone cold wakes (cf. Fig. 9a to Fig. 6b). Consistently with Fig. 6b, the analytical approach suggests that the strongest effect of rainfall is found in the Arabian Sea (median of −0.15 K) and in the south Indian Ocean (median of −0.10 K). All other basins display smaller effects $O(-0.06$ K).

Equation (11) links the effect of rainfall to the approximate MLD, after the cyclone $\mathcal{H}_m$, to the rainfall buoyancy flux $\mathcal{B}$ and to the contribution of temperature to stratification $\alpha a/\tilde{N}^2$. The distribution of these values is provided in Figs. 9b,c,d. As seen in Fig. 9b, the strongest rainfall-induced buoyancy fluxes, that is, the strongest precipitation within cyclones are found in the Arabian Sea and Bay of Bengal (median p of 13.2 and 14.9 cm, respectively). The distributions of $\mathcal{H}_m$ are similar in most basins (i.e., have close median values between 65 and 75 m) except in the northeastern Pacific where $\mathcal{H}_m$ is about 45 m. Those smaller values of $\mathcal{H}_m$ are not related to the TC wind stress power, which is quite strong in the northeast Pacific, but rather to the oceanic stratification there [see Fig. 1b, and Vincent et al. (2012b) in particular their Figs. 3a and 3d]. Finally, the contribution of temperature to stratification is lowest in the very salt-stratified Bay of Bengal (median of 0.43), known for its

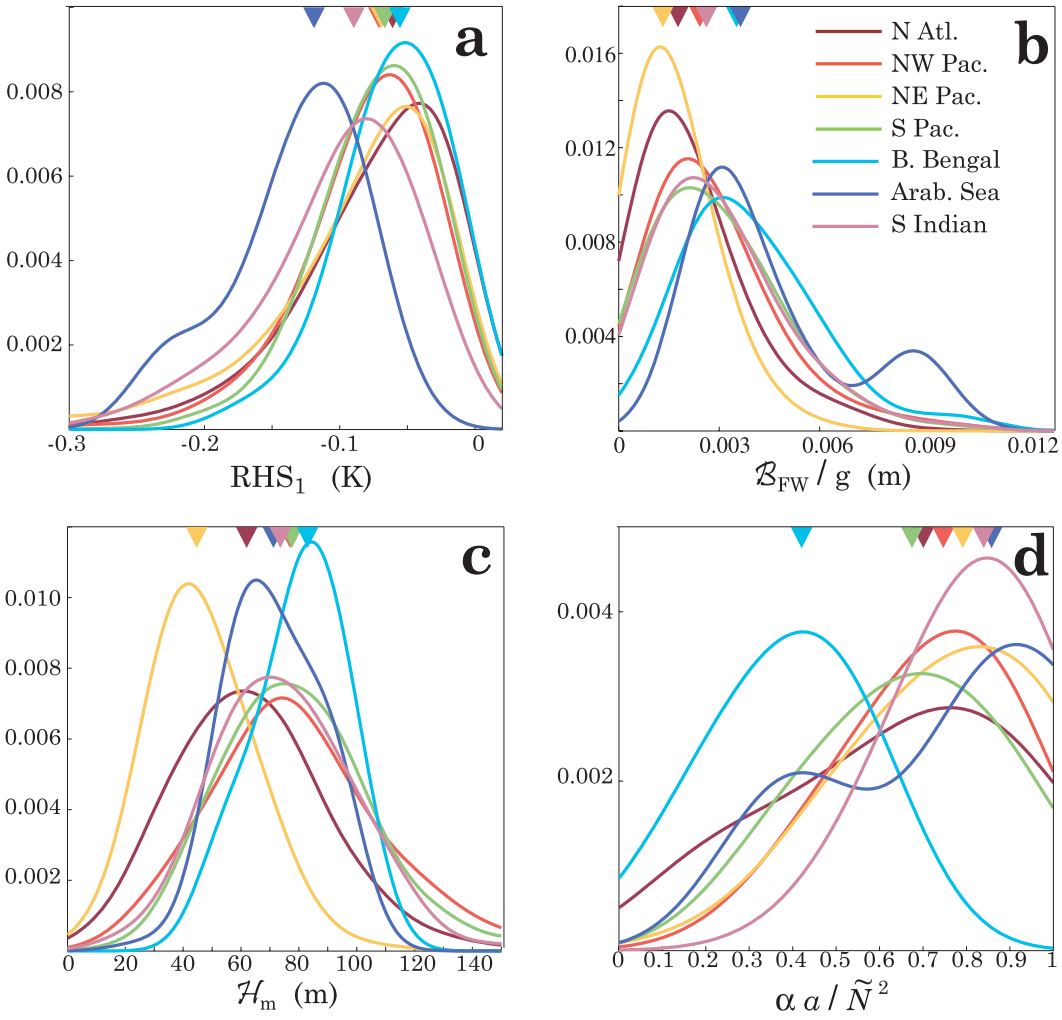

FIG. 9. PDF of (a) RHS_1, (b) $\mathcal{B}_{FW}/g$, (c) $\mathcal{H}_m$, and (d) $\alpha a/\tilde{N}^2$. Color triangles indicate the median related to each PDF. The PDFs are computed by attributing identical Gaussian functions to every value and adding them up.

thick barrier layer after the monsoon (see also Fig. 1c). There is an intermediate contribution of thermal stratification (around 0.65 to 0.7) in the South Pacific, North Atlantic and northwest Pacific. The thermal stratification is strongest (median 0.8 to 0.85) in the northeastern Pacific, south Indian Ocean, and Arabian Sea.

In the Arabian Sea, the strong rainfall within cyclones (Fig. 9b), combined with a strong contribution of temperature to the density stratification (Fig. 9d), explain the larger influence of rainfall on the cold wake than in other basins. The rainfall buoyancy flux within cyclones is also strong in the Bay of Bengal (Fig. 9b), but the very strong haline stratification (Fig. 9d) results in one of the weakest rainfalls influencing the cold wake (Fig. 9a). The shallow $\mathcal{H}_m$ in the the northeastern Pacific (Fig. 9c) is counterbalanced by quite weakly precipitating cyclones (Fig. 9b), also resulting in a weak rainfall influence on the cold wake (Fig. 9a). The south Indian cyclonic basin comes out as the second-ranking effect of rainfall on the cold wake because of the combined influence of relatively intense precipitation within cyclones (Fig. 9b) and a strong thermal stratification (Fig. 9d).

5. Discussion and conclusions

a. Summary

Ocean surface cooling induced by tropical cyclones can inhibit their intensification. A thorough understanding of the mechanisms controlling this cooling is thus needed to better account for the influence of air–sea interactions on TC intensity in forecasting systems. In this study, we have specifically investigated the influence of heavy rainfall associated with TCs on the amplitude of the cold wake at global scale, using observation-based products. Our study covers the 2002–09 period and includes

analysis of the rainfall effect on TC-induced cooling for more than 800 observed cyclones. Along each of these TC tracks, surface cooling and the accumulated precipitation have been derived from satellite data, while precyclone stratification has been obtained from GLORYS2 ocean reanalysis. Using these estimates and assuming that cooling is entirely due to vertical mixing, we have estimated the postcyclone temperature and salinity profile in the presence of rainfall.

A first interesting result is that salinity usually increases in the wake of cyclones because vertical mixing entrains subsurface water that is, on average, saltier than surface water in convective regions associated with cyclonic activity. This mixing effect overwhelms the dilution effect of rain freshwater: the cyclone ''cold wake'' is hence also generally a ''salty wake.''

Then, we have developed a method for estimating the effect of rainfall on the cold wake. Our physical assumption considers that an extra quantity of energy (corresponding to the potential energy change of the rain layer in the case it is mixed into the ocean) is available for mixing the ocean column in the hypothetical case with no rain. Assuming a linearly stratified ocean, we have derived an analytical solution whose results agree well with the complete numerical solution. This analytical formulation gives an insight into the factors controlling the rainfall effect on cooling and their regional variations.

The stabilizing effect of rainfall tends to reduce the postcyclone mixing depth and, hence reduces the cooling. Reduction of the mixing depth due to the stabilizing effect of rainfall diminishes cooling under TCs by a small amount (median of 0.07 K versus a median 1 K cold wake). The temperature of rainfall (i.e., rain sensible flux) has a negligible effect. Rainfall has the largest impact in the Arabian Sea (median of 0.15 K versus a median 1.4 K cold wake) compared to the other TC-prone basins. The impact is largest in the Arabian sea owing to the combination of strong rainfall (and hence a strong stabilizing effect) and a strong thermal stratification (the mixing depth reduction hence significantly reduces the entrainment cooling). By contrast, the Bay of Bengal displays a smaller effect of rainfall on the cold wake because of the presence of a strong barrier layer. The overall effect of rainfall is, hence, overall quite weak (median of 7%), though not negligible: it reduces the cooling by 19% or more for 10% of the cases. For some particular cases, it can be as strong as 0.3 K.

b. Limits of the datasets used in this study

We now provide a brief discussion of our results, starting with uncertainties arising from the products that we use.

We have assumed that the cold wake is adequately captured by the TMI-AMSRE dataset. Estimating the uncertainty on (ΔSST_{obs}) is difficult. But, the fact that the fully independent modeling results of Vincent et al. (2012b) display a good overall agreement with TMI-AMSRE provides some indication that TMI-AMSRE somewhat captures the cold wake. Moreover, the masking effect of the cold wake by heavy rainfall is likely to have a small impact on the estimation of (ΔSST_{obs}) because the cold wake has been monitored 2 to 3 days after cyclone passage, that is, after the most intense precipitating systems. We also rely on the TRMM 3B42 rainfall value to estimate the effect of rainfall on the cold wake. Chen et al. (2012, manuscript submitted to *J. Geophys. Res.*) have compared TC rainfall from 3B42 to 365 surface gauge records in oceanic conditions. They have estimated that 3B42 overestimates TC rainfall by 14% on average. This may induce a slight overestimate of the effect of rainfall in our study.

There is also an uncertainty in the estimate of the oceanic temperature and salinity profiles that we use (Figs. 3a,b). When an Argo profile is assimilated into GLORYS, the relative uncertainty on estimated linear slopes a and b is 4% and 0.8%, respectively (Figs. 3c,d). The ratio of TC occurrences for which at least one in situ measurement has been made in the 10 days prior to the TC passage, in a disk of 2° radius, is ~23% in the first 100 m. Between these measurements, we rely on the model physics, which has been shown to capture an accurate oceanic state without data assimilation (Penduff et al. 2010 and references therein). To have a better insight on the uncertainty related to the use of GLORYS2, we have repeated all of the analysis in this paper using the GLORYS1 reanalysis (Ferry et al. 2010) instead of GLORYS2. Despite numerous differences between GLORYS1 and GLORYS2 (parameterizations of the ocean model, assimilated data, atmospheric forcing), all the results presented are very similar to that obtained from GLORYS1, the median value of the rainfall effect on ΔSST is also a cooling inhibition by 0.07 K, and the regional contrasts are the same (not shown).

If the uncertainties above are assumed to be independent from each other (i.e., square relative uncertainties add up), the uncertainty on our estimate can be inferred from Eq. (11): a relative uncertainty of 20% on both p and $(\Delta SST)_{obs}$ would lead to about 30% relative uncertainty on our estimate. We hence consider that our statement that the overall impact of rainfall is generally relatively small (about 10% of the observed cooling) is quite robust.

c. Discussion of the physical hypotheses

The first limit to our approach is that we assume that the cooling is entirely due to mixing. Vincent et al. (2012b)

show that about 80% of the cooling may be due to mixing for the strongest and slowest cyclones. This fraction is reduced to 30% for the weakest and fastest TCs. From a physical perspective, we expect rainfall to influence much more vertical mixing than air–sea fluxes or lateral advection. The approach taken in this paper is hence probably valid but should be applied to the part of observed cooling $(\Delta SST)_{obs}$ that can be attributed to mixing—between 50% and 80% depending on the cyclone power. Including such a dependency would probably tend to diminish the relative effect of rainfall and would, hence, probably not affect our main statement that the effect of rainfall is on average relatively small.

Our second major assumption is that the system {ocean + rain} undergoes the same potential energy change ΔE_p as the system {ocean} in the absence of rainfall; that is, an extra quantity of energy (corresponding to the potential energy change of the rain layer in the case it is mixed into the ocean) is available for mixing the ocean column in the hypothetical case with no rain. The complete physics of mixed layer dynamics in the presence of strong rainfall are hence not accounted for in our methodology. The buoyancy flux associated with rainfall will, indeed, act to increase vertical stratification, trap momentum near the surface, and increase vertical shear in the early stages of the cyclones. This can both affect the amount of kinetic energy transferred by the cyclone to the ocean (which is computed as the time-integral of the scalar product of wind stress and surface currents, and hence depends on surface currents), and on turbulence generation (which will be favored by stronger shear but damped by stronger stratification). It is not straightforward to anticipate how these various effects will be compensated.

Moreover, evaporation is neglected in the salt and buoyancy budgets in this paper. Little evaporation occurs within a disk of ~1° (Cione et al. 2000) because air is near saturation and most of the moisture feeding atmospheric convection is advected from as far as 1600 km from the eye (Trenberth et al. 2007). To estimate evaporation within our disks of 2° radius, we have analyzed outputs from a 1/3° interannual ocean simulation from the regional ocean modeling system (ROMS) model (Jullien et al. 2012), two-way coupled to an equivalent atmospheric configuration from the Weather Research and Forecasting (WRF) model (Jourdain et al. 2011). The total evaporation e during the TC passage is well described by the linear relationship $e = 0.23p$. Once again, including evaporation would result in a slight reduction (23%) of the effect of rainfall on the cold wake, and this would not affect our main conclusion that this effect is on average relatively weak.

Another limit to our approach is the assumption that vertical advection does not influence the ocean response. First, upwelling under TCs tends to increase the efficiency of vertical mixing by lifting the thermocline. This is somehow taken into account in our methodology because we consider the observed cooling to estimate vertical mixing (i.e., we consider mixing strengthened by the the presence of an upwelling).

Finally, we assume that the mixed layer is perfectly homogenous, and results would probably be slightly different using a more elaborate mixing scheme (Jacob and Koblinsky 2007). The issue is that such a scheme would require an accurate description of the wind field for each TC, and directly deriving the influence of rainfall from the observed SST is a major strength of our approach.

Acknowledgments. The research leading to this study received support from: the European Community's Seventh Framework Programme FP7/2007-2013 under Grant Agreement 218812 (MyOcean), the project Les Enveloppes Fluides et l'Environnement (LEFE) CYCLOCEAN AO2010-538863, the national programme GMMC (Groupe Mission Mercator Coriolis), and the Institut National des Sciences de l'Univers (INSU). The authors gratefully thank the team Mercator-Ocean who provided the ocean reanalysis GLORYS1 and GLORYS2, as well as Mélanie Juza who provided the ARGO-reanalysis colocation tools. ML, JV, CM, EV, and GS were supported by Institut de Recherche pour le Developpement (IRD) funding. BB and GM were supported by Centre National de la Recherche Scientifique (CNRS).

REFERENCES

Agence France-Presse, cited 2003: Philippines: Typhoon Linfa downgraded to temperate depression, bringing heavy rainfall. [Available online at http://reliefweb.int/node/127324.]

Anderson, S. P., A. Hinton, and R. A. Weller, 1998: Moored observations of precipitation temperature. *J. Atmos. Oceanic Technol.,* **15,** 979–986.

Balaguru, K., P. Chang, R. Saravanan, L. R. Leung, Z. Xu, M. Li, and J. S. Hsieh, 2012: Ocean barrier layers effect on tropical cyclone intensification. *Proc. Natl. Acad. Sci.,* **109,** 14 343–14 347.

Bender, M., and I. Ginis, 2000: Real-case simulations of hurricane–ocean interaction using a high-resolution coupled model: Effects on hurricane intensity. *Mon. Wea. Rev.,* **128,** 917–946.

Chang, S. W., and R. A. Anthes, 1978: Numerical simulations of the ocean's nonlinear baroclinic response to translating hurricanes. *J. Phys. Oceanogr.,* **8,** 468–480.

Cione, J. J., and E. W. Uhlhorn, 2003: Sea surface temperature variability in hurricanes: Implications with respect to intensity change. *Mon. Wea. Rev.,* **131,** 1783–1796.

——, P. G. Black, and S. H. Houston, 2000: Surface observations in the hurricane environment. *Mon. Wea. Rev.,* **128,** 1550–1561.

Collecte Localisation Satellites, 2011: SSALTO/DUACS user handbook CNES/IFREMER Tech. Rep CLS-DOS-NT-06-034, 2rev5, 70 pp. [Available online at http://www.aviso.oceanobs.com/fileadmin/documents/data/tools/hdbk_duacs.pdf.]

Crawford, G. B., and W. G. Large, 1996: A numerical investigation of resonant inertial response of the ocean to wind forcing. *J. Phys. Oceanogr.,* **26,** 873–891.

D'Asaro, E. A., 1985: The energy flux from the wind to near-inertial motions in the surface mixed layer. *J. Phys. Oceanogr.,* **15,** 1043–1059.

——, C. C. Eriksen, M. D. Levine, P. Niiler, C. A. Paulson, and P. Van Meurs, 1995: Upper-ocean inertial currents forced by a strong storm. Part I: Data and comparisons with linear theory. *J. Phys. Oceanogr.,* **25,** 2909–2936.

——, T. B. Sanford, P. P. Niiler, and E. J. Terrill, 2007: Cold wake of Hurricane Frances. *Geophys. Res. Lett.,* **34,** L15609, doi:10.1029/2007GL030160.

de Boyer Montégut, C., G. Madec, A. Fischer, A. Lazar, and D. Iudicone, 2004: Mixed layer depth over the global ocean: An examination of profile data and a profile-based climatology. *J. Geophys. Res.,* **109,** C12003, doi:10.1029/2007GL030160.

Dee, D. P., and Coauthors, 2011: The ERA-Interim reanalysis: Configuration and performance of the data assimilation system. *Quart. J. Roy. Meteor. Soc.,* **137,** 553–597.

DeMaria, M., M. Mainelli, L. K. Shay, J. A. Knaff, and J. Kaplan, 2005: Further improvements to the statistical hurricane intensity prediction scheme (SHIPS). *Wea. Forecasting,* **20,** 531–543.

——, J. Knaff, and C. Sampson, 2007: Evaluation of long-term trends in tropical cyclone intensity forecasts. *Meteor. Atmos. Phys.,* **97,** 19–28.

Emanuel, K., 2000: A statistical analysis of tropical cyclone intensity. *Mon. Wea. Rev.,* **128,** 1139–1152.

Ferry, N., and Coauthors, 2010: Mercator global eddy permitting ocean reanalysis GLORYS1V1: Description and results. *Mercator Quarterly Newsletter,* No. 36, Mercator Ocean Office, Toulouse, France, 15–27.

——, and Coauthors, 2012: GLORYS2V1 global ocean reanalysis of the altimetric era (1993-2009) at mesoscale. *Mercator Quarterly Newsletter,* No. 44, Mercator Ocean Office, Toulouse, France 28–39.

Gill, A. E., 1982: *Atmosphere-Ocean Dynamics.* Academic Press, 662 pp.

Godfrey, J. S., and E. J. Lindstrom, 1989: The heat budget of the equatorial western Pacific surface mixed layer. *J. Geophys. Res.,* **94** (C6), 8007–8017.

Gosnell, R., C. Fairall, and P. Webster, 1995: The sensible heat of rainfall in the tropical ocean. *J. Geophys. Res.,* **100** (C9), 18 437–18 442.

Greatbatch, R. J., 1983: On the response of the ocean to a moving storm: The nonlinear dynamics. *J. Phys. Oceanogr.,* **13,** 357–367.

——, 1984: On the response of the ocean to a moving storm: Parameters and scales. *J. Phys. Oceanogr.,* **14,** 59–78.

Hu, A. and G. A. Meehl, 2009: Effect of the Atlantic hurricanes on the oceanic meridional overturning circulation and heat transport. *Geophys. Res. Lett.,* **36,** L03702, doi:10.1029/2008GL036680.

Ingleby, B., and M. Huddleston, 2007: Quality control of ocean temperature and salinity profiles Historical and real-time data. *J. Mar. Syst.,* **65,** 158–175.

Jackett, D. R., and T. J. McDougall, 1995: Minimal adjustment of hydrographic profiles to achieve static stability. *J. Atmos. Oceanic Technol.,* **12,** 381–389.

Jacob, S. D., and C. Koblinsky, 2007: Effects of precipitation on the upper-ocean response to a hurricane. *Mon. Wea. Rev.,* **135,** 2207–2225.

——, L. K. Shay, A. J. Mariano, and P. G. Black, 2000: The 3D oceanic mixed layer response to Hurricane Gilbert. *J. Phys. Oceanogr.,* **30,** 1407–1429.

Jiang, H., and E. J. Zipser, 2010: Contribution of tropical cyclones to the global precipitation from 8 seasons of TRMM data: Regional, seasonal, and interannual variations. *J. Climate,* **23,** 1526–1543.

Jourdain, N. C., P. Marchesiello, C. E. Menkes, J. Lefvre, E. M. Vincent, M. Lengaigne, and F. Chauvin, 2011: Mesoscale simulation of tropical cyclones in the South Pacific: Climatology and interannual variability. *J. Climate,* **24,** 3–25.

Jullien, S., and Coauthors, 2012: Impact of tropical cyclones on the heat budget of the South Pacific Ocean. *J. Phys. Oceanogr.,* **42,** 1882–1906.

Juza, M., T. Penduff, J. M. Brankart, and B. Barnier, 2012: Estimating the distortion of mixed layer property distributions induced by the Argo sampling. *J. Oper. Oceanogr.,* **5,** 45–58.

Kaplan, J., and M. De Maria, 2003: Large-scale characteristics of rapidly intensifying tropical cyclones in the North Atlantic basin. *Wea. Forecasting,* **18,** 1093–1108.

Knapp, K. R., M. C. Kruk, D. H. Levinson, H. J. Diamond, and C. J. Neumann, 2010: The international best track archive for climate stewardship (IBTrACS). *Bull. Amer. Meteor. Soc.,* **91,** 363–376.

Levy, M., and Coauthors, 2012: Contribution of tropical cyclones to the air-sea CO2 flux: A global view. *Global Biogeochem. Cycles,* **26,** GB2001, doi:10.1029/2011GB004145.

Lloyd, I., and G. Vecchi, 2011: Observational evidence for oceanic controls on hurricane intensity. *J. Climate,* **24,** 1138–1153.

Madec, G., 2008: NEMO ocean engine. Institut Pierre-Simon Laplace Tech. Rep. Note du Pôle de Modelisation 27, 367 pp.

Mainelli, M., M. DeMaria, L. K. Shay, and G. Goni, 2008: Application of oceanic heat content estimation to operational forecasting of recent Atlantic category 5 hurricanes. *Wea. Forecasting,* **23,** 3–16.

Marks, F. D., and L. K. Shay, 1998: Landfalling tropical cyclones: Forecast problems and associated research opportunities. *Bull. Amer. Meteor. Soc.,* **79,** 305–323.

Neetu, S., M. Lengaigne, E. M. Vincent, J. Vialard, G. Madec, G. Samson, M. R. Ramesh Kumar, and F. Durand, 2012: Influence of upper-ocean stratification on tropical cyclone-induced surface cooling in the Bay of Bengal. *J. Geophys. Res.,* doi:10.1029/2012JC008433, in press.

Penduff, T., M. Juza, L. Brodeau, G. Smith, B. Barnier, J. Molines, A. Treguier, and G. Madec, 2010: Impact of global ocean model resolution on sea-level variability with emphasis on interannual time scales. *Ocean Sci.,* **6,** 269–284.

Price, J. F., 1981: Upper-ocean response to a hurricane. *J. Phys. Oceanogr.,* **11,** 153–175.

——, 1983: Internal wave wake of a moving storm. Part I: Scales, energy budget, and observations. *J. Phys. Oceanogr.,* **13,** 949–965.

——, 2009: Metrics of hurricane-ocean interaction: Vertically-integrated or vertically-averaged ocean temperature? *Ocean Sci.,* **5,** 351–368.

——, T. B. Sanford, and G. Z. Forristall, 1994: Forced stage response to a moving hurricane. *J. Phys. Oceanogr.,* **24,** 233–260

Samson, G., H. Giordani, G. Caniaux, and F. Roux, 2009: Numerical investigation of an oceanic resonant regime induced by hurricane winds. *Ocean Dyn.,* **59,** 565–586.

Schade, L. R., 2000: Tropical cyclone intensity and sea surface temperature. *J. Atmos. Sci.,* **57,** 3122–3130.

——, and K. A. Emanuel, 1999: The ocean's effect on the intensity of tropical cyclones: Results from a simple coupled atmosphere–ocean model. *J. Atmos. Sci.,* **56,** 642–651.

Shay, L. K., R. L. Elsberry, and P. G. Black, 1989: Vertical structure of the ocean current response to a hurricane. *J. Phys. Oceanogr.,* **19,** 649–669.

——, P. Black, A. Mariano, J. Hawkins, and R. Elsberry, 1992: Upper ocean response to Hurricane Gilbert. *J. Geophys. Res.,* **97** (C12), 20 227–20 248.

Simmons, A., S. Uppala, D. Dee, and S. Kobayashi, 2007: ERA-Interim: New ECMWF reanalysis products from 1989 onwards. *ECMWF Newsletter,* No. 110, ECMWF, Reading, United Kingdom, 25–35.

Sprintall, J., and M. Tomczak, 1992: Evidence of the barrier layer in the surface layer of the tropics. *J. Geophys. Res.,* **97** (C5), 7305–7316.

Trenberth, K. E., C. A. Davis, and J. Fasullo, 2007: Water and energy budgets of hurricanes: Case studies of Ivan and Katrina. *J. Geophys. Res.,* **112,** D23106, doi:10.1029/2006JD008303.

Troccoli, A., and P. Kållberg, 2004: Precipitation correction in the ERA-40 reanalyses. European Centre for Medium-Range Weather Forecasts, ERA-40 Project Report Series 13, 6 pp.

Tsai, Y., C. Chern, and J. Wang, 2008: The upper ocean response to a moving typhoon. *J. Oceanogr.,* **64,** 115–130.

Verbrugge, N., and G. Garric, 2010: Large scale ECMWF radiative surface fluxes assessment, correction and application to 3D-global Ocean simulations. *Proc. EGU General Assembly,* Vienna, Austria, EGU, 12044.

Vincent, E. M., M. Lengaigne, G. Madec, J. Vialard, G. Samson, N. C. Jourdain, C. E. Menkes, and S. Jullien, 2012a: Processes setting the characteristics of sea surface cooling induced by tropical cyclones. *J. Geophys. Res.,* **117,** C02020, doi:10.1029/2011JC007396.

——, ——, J. Vialard, G. Madec, N. C. Jourdain, and S. Masson, 2012b: Assessing the oceanic control on the amplitude of sea surface cooling induced by tropical cyclones. *J. Geophys. Res.,* **117,** C05023, doi:10.1029/2011JC007705.

Wentz, F., C. Gentemann, D. Smith, and D. Chelton, 2000: Satellite measurements of sea surface temperature through clouds. *Science,* **288,** 847–850.